

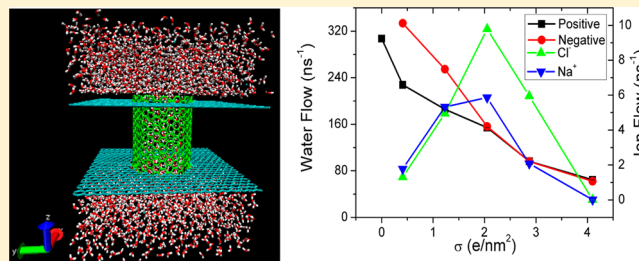
Water Permeation Through a Charged Channel

Liang Hao, Jiaye Su,* and Hongxia Guo*

Beijing National Laboratory for Molecular Sciences, Joint Laboratory of Polymer Sciences and Materials, State Key Laboratory of Polymer Physics and Chemistry, Institute of Chemistry, Chinese Academy of Sciences, Beijing 100190, China

S Supporting Information

ABSTRACT: Transport properties of water molecules through hydrophobic channels have been explored extensively in recent years; however, our knowledge about the transport properties of hydrophilic channels is still rather poor. Herein, we use molecular dynamics simulations to study the permeation of water molecules through a charged channel. For comparison, we first consider the pristine hydrophobic channel without charge, and we find an analytic expression that can predict the water flow through it. For uniformly charged channels, with the increase of charge density, the water flow decreases, due to the increase of roughness in the free energy profile experienced by a water molecule along the channel; while the ion flow exhibits a maximum, because of the competition between the increasing ion number and ion-channel attraction. Surprisingly, the water occupancy for positive and negative channels varies in the opposite direction, which is strongly related to the excluded volume effect of ions. Additionally, we also discuss the effect of surface charge patterns and channel sizes. These results not only enrich our understanding of the transport properties of hydrophilic channels, but also have deep implications for the design of nanometer water gates.



1. INTRODUCTION

The phenomenon of fluid transport in narrow channels is not only relevant to our daily life but also crucial to life itself, e.g., water and ions are selectively and efficiently transported in and out of cells by protein channels. It has been recognized that the specific functions of protein channels are determined by their charged residues.^{1–3} As an ideal, robust, and controllable model system with well-defined structures, carbon nanotube (CNT) exhibits huge superiority as a fast water transporter, confirmed by both experiments^{4,5} and simulations.^{6,7} It is believed that the rapid conduction of water inside CNTs is strongly coupled to their unique structure and stronger hydrogen bonds than bulk water, as well as weak water–CNT interactions.⁸ The confined water can form a single-file arrangement inside a subnanometer CNT^{6,9–11} and ordered ice–tube structures in wider CNTs,^{12,13} which are observed by recent experiments.^{14–16} The water flow enhancement is found to be dependent on these water structures or CNT diameters.^{17,18} In addition, understanding the transport properties of water through CNTs is not only a pure lab on a chip interest, but also relevant to the design of novel nanofluidic devices, including desalination machines,^{19,20} molecular sieves,^{21,22} drug delivery,²³ biosensors,²⁴ as well as water gates.²⁵

It has been shown that the transport of water through CNTs is a complex process and often affected by many factors, such as temperatures,^{15,26} pressures,¹⁷ and electric fields.^{26,27} Although great effort has been made during the past decades, most of the work considered pure hydrophobic channels,^{6–18} while little is known of the transport properties in hydrophilic channels. As aforementioned, charged residues inside protein channels

control the transport and selectivity of water and ions, and even change water dipole orientations.¹ Thus it can be expected that, even for a hydrophobic channel, the transport of water or ions should be sensitive to the charges inside or outside the channel. From this perspective, some recent simulation studies have moved to the design of a novel nanofluidic channel based on CNTs by adding charged residues. Examples include ion filters or sieves,^{3,21} desalination devices,¹⁹ water gates,²⁵ and artificial water channels,²⁸ where charged residues have been proven to play a very important role in determining the dynamics of water and ions. Meanwhile, experimental work has shown that for a homogeneously charged channel, the surface charge governs the transport of ions.^{29–33} Actually, the counterions inside the charged channel form an electric double layer (EDL), exhibiting counterion selectivity. Thus it can be expected that the surface charge density and patterns will have a profound impact on the transport of water molecules.

Despite charged channels having been investigated extensively in experiments,^{29–33} theoretical studies are exceedingly rare. In recent simulation work, charged channels with different patterns were considered to investigate the pressure-driven transport of water and salt solutions, where the salt rejection and salt flux rectification dependent on size and structure are addressed.³⁴ Alternatively, Melillo et al performed molecular dynamics simulations (MD) and changed the channel hydrophilicity by varying the water–channel hydrophobic interactions

Received: January 17, 2013

Revised: May 26, 2013

Published: June 6, 2013

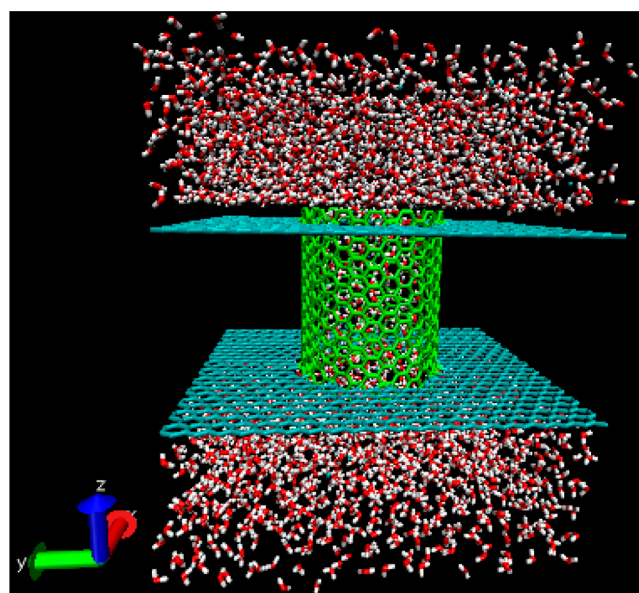
instead of adding charges, and found enhanced water flow with the increase of water-channel interactions.³⁵ Similar MD work reported the importance of water-channel interaction in the water transportation.^{36,37} Hence, hydrophilic channels could exhibit very different transport properties from hydrophobic ones, which not only inspires pure scientific interest but also is crucial to the design of nanofluidic devices. However, to the best of our knowledge, how water molecules transport through a hydrophilic channel has not yet been understood clearly, especially the relation between water flow and surface charge density or patterns.

2. MODEL AND SIMULATION METHODS

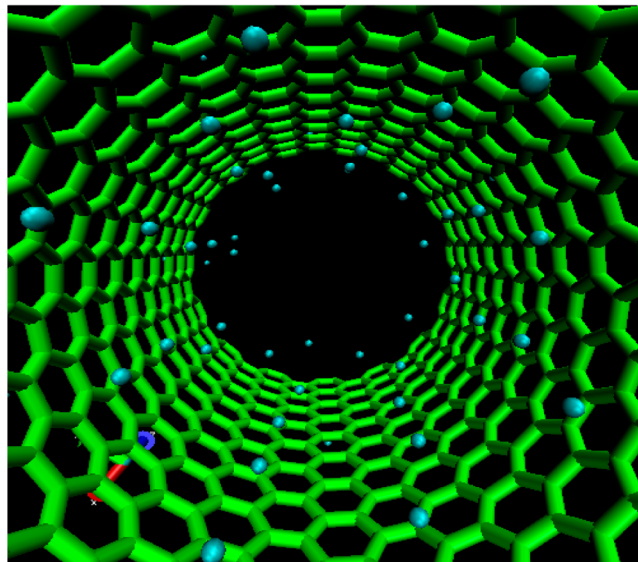
In the present work, we used MD simulations to study the conduction of water molecules through charged CNT channels with various patterns. Figure 1(a) shows a snapshot of the simulation system, where the box size is about $5.1 \times 5.1 \times 6.1$ nm³, containing 3136 water molecules. The two membrane sheets are electrically neutral and the CNT channel (green) is positively (or negatively) charged. The channel with diameter and length around 2.02 and 2.56 nm, respectively, which corresponds to nanotube (15,15), is considered as the main simulated system. We chose this wide channel in order to ensure that inside the channel the counterions have enough space to form complete electrical double layer (EDL), while the water structures are close to those in the bulk state, which can be considered as a general case, comparable to experimental charged channels.^{29–33}

We first considered the channels that are homogeneously charged, and we changed the surface charge density σ for a range of 0.41–4.1 e/nm². In some recent experiments,^{29–33} the charge density of channels was set as high as 1–2 e/nm². Thus our considered density values are close to those of real fabricated channels. Then we investigated the distribution of charges while keeping the total amount as $\sigma = 2.05$ e/nm², similar to previous consideration for charged nanoparticles.³⁸ Figure 1(b) gives the distribution of counterions (either Cl[−] or Na⁺) inside the channel. The counterions can be strongly adsorbed onto the interior surface at high charge density and form electrical double layer (EDL), which then determines the permeation of water molecules. Detailed charge patterns can be found in our Supporting Information. In addition to this main channel system, for the fixed charge density of $\sigma = 2.05$ e/nm², we further considered four other smaller ones with the same length, whose diameters are 0.81, 1.08, 1.35, and 1.62 nm, corresponding to nanotubes (6,6), (8,8), (10,10), and (12,12), respectively. The major goal of the current study is to elucidate the effect of surface charge density and its patterns, as well as the channel size on the transport dynamics of water molecules.

All MD simulations were carried out at constant volume and temperature (300 K) using the Nose-Hoover method for temperature coupling with Gromacs 3.3.1 simulation package.³⁹ The TIP3P water model was used.⁴⁰ Known carbon–carbon and carbon–water interaction parameters⁶ and ion parameters⁴¹ were used. The particle-mesh Ewald method was used to treat the long-range electrostatic interactions.⁴² Periodic conditions were applied in all directions. A time-step of 2 fs was used, and data were collected every 0.5 ps. A damping time of 0.1 ps was used, which is 50 times larger than the time-step. According to a recent work,⁴³ damping time in the Nose-Hoover thermostat that is too short will result in large frictions that reduce the diffusion ability. Thus, the viable damping time is suggested to be 40 times larger than the time-step. Our



(a)



(b)

Figure 1. (a) Snapshot of the simulation system, where the box size is about $5.1 \times 5.1 \times 6.1$ nm³. The two membrane sheets are charge neutral and the channel (green) is positively (or negatively) charged. The channel diameter and length are 2.02 and 2.56 nm, respectively. (b) Inside the channel, the counterions (Cl[−]) are adsorbed onto the interior surface, forming an electrical double layer (EDL).

damping time of 0.1 ps is in accord with this criteria, and can control the system temperature well and reproduce the bulk properties of TIP3P water. The CNT channel combined with two graphite sheets were held fixed during the simulations. For each charge density, charge pattern, and channel diameter, we conducted two independent 130 ns MD runs, and the last 125 ns trajectory was used for data analysis. Standard error bars were estimated over these two independent data.

3. RESULTS AND DISCUSSION

3.1. Uncharged Channel. Following previous work,^{6,9,18,25,27} we define the water flow as the total number of water molecules per nanosecond leaving one end of the

CNT channel that previously entered the other end. For comparison, we first conducted MD runs for the case of a pristine CNT (15,15) channel without charge modification. For the two 125 ns MD trajectories we counted 38452 and 38368 water molecules that are conducted through the channel, respectively, resulting in $307.3 \pm 0.5 \text{ ns}^{-1}$ water flow. Actually, since we do not apply any external force to drive water transport, the water flow can be considered a purely diffusive flow. Generally, we can consider the water flow through a given volume V as

$$Q = \int_S n u \, ds \quad (1)$$

where S is the channel cross section. n is the number density of water, and u is the velocity of water along the channel direction. The one-dimensional diffusion equation for conventional translational motion can be written as

$$\langle \Delta z^2 \rangle = 2Dt \quad (2)$$

where D is the diffusion coefficient of bulk water. As the water structure inside the current wide channel is similar to that of bulk water, the diffusion coefficient can also be assumed to be the same. Thus for an individual water molecule, on average, the duration of its diffusion from one channel end to the other is $t_d \approx L^2/2D$. The mean velocity of water molecules inside the channel should be $\bar{u} \approx 2D/L$. Although for each water molecule inside the channel, its velocity should be time- and space-dependent, we are concerned about its mean contribution to the water flow. Therefore, we can replace the individual velocity in eq 1 by the mean velocity and we have

$$Q = \frac{2D}{L} \int_S n \, ds \quad (3)$$

where the result of integration in the right-hand side is clearly the number of water occupancy at a given channel cross section. Thus we finally obtain the flow as

$$Q = \frac{2D}{L^2} \langle N_w \rangle \quad (4)$$

where $\langle N_w \rangle$ is the water occupancy inside the channel. For the TIP3P water, according to Yeh and Hummer,⁴⁴ the large-system limit for D is $\sim 6.05 \text{ nm}^2/\text{ns}$. We conducted a 12 ns MD run for a periodic water box containing 3375 water molecules, and obtained the bulk diffusion coefficient as $D = 5.856 \text{ nm}^2/\text{ns}$. For comparison with the current simulated water flow, containing 3136 waters, it is reasonable to use $D = 5.856 \text{ nm}^2/\text{ns}$. We counted the water occupancy as $\langle N_w \rangle = 180.6 \pm 0.03$. Finally, from eq 4 the predicted water flow is $Q = 322.8 \text{ ns}^{-1}$, which is close to our simulation results of $307.3 \pm 0.5 \text{ ns}^{-1}$. Consequently, eq 4 can give a reasonable prediction of water flow through hydrophobic channels. We can understand eq 4 as that, during the diffusion duration of t_d , the number of water molecules flowing through the channel is equal to the occupancy. Similarly, Melillo et al. presented a linear relation of water flow vs $\langle N_w \rangle/\tau_w$ directly from their simulation results,³⁵ where the proportionality constant is 0.36.

According to the bulk water diffusion coefficient of $D = 5.856 \text{ nm}^2/\text{ns}$, $t_d \approx L^2/2D$ is equal to about 560 ps, while the translocation time extracted from MD trajectory is $\tau_w = 1171 \pm 16 \text{ ps}$. Clearly, if we use τ_w for estimation, the flow of $Q = \langle N_w \rangle/\tau_w = 154.2 \text{ ns}^{-1}$, is about half of the prediction by $\langle N_w \rangle/t_d$. The origin of these differences can be traced back to the fact

that although the translocation times of most water molecules are only several hundreds of picoseconds, some water molecules have large values. For example, for the 250 ns (two independent 125 ns) MD trajectory, the total number of water molecules flowing through the channel is 76820, where only 1180 (1.54% of total) have τ_w larger than 20 ns. Excluding these 1180 water molecules, the average τ_w can be reduced to 658 ps. That is to say, the average value of τ_w is susceptible to the small portion of water that have large τ_w . Since most water inside our current wide CNT are in the fluid phase and are expected to display linear diffusion, it is reasonable to use $t_d \approx L^2/2D$ in general predictions. On the other hand, the results of Hummer et al.⁶ and Kofinger et al.¹⁰ indicated that the fast water flow through narrow CNTs is due to the formation of stronger hydrogen-bonds than those in bulk water and the collective motion of the single-file water chain. However, the case may be different from wider CNT situations, as evidenced by the decrease of flow enhancement with the increase of CNT diameter.¹⁷ For our current wide CNT, the water structure inside is close to the bulk state; thus, we suggest a simple diffusion model which would predict the water flow, to a certain extent, close to that obtained in simulations and will elucidate this issue further in future studies.

In general, the liquid diffusion on a solid interface should be different from bulk diffusive behavior due to the liquid–solid interactions. In a recent work, Milischuk et al. studied the structure and dynamics of water confined in silica nanopores and found that the water molecules close to the silica surface have lower mobility than those in the pore center or bulk.⁴⁵ A similar conclusion was drawn by Cheng et al. in their study of acetonitriles confined in silica pores.⁴⁶ This difference may also depend on pore diameters. Thus, it will be interesting to investigate this question systematically for different CNT diameters, and further explore the difference in the water flow estimated from the diffusion constant and the average translocation time. However, it will need large amounts of MD runs and elaborate analysis. As the current work focuses on the effect of charge density and patterns on the water permeation, we will explore these questions in future work, where we can evaluate eq 4 in more detail for different CNT diameters and/or lengths.

In addition, it is often suggested that the water occupancy should be proportional to channel volume, i.e., $\langle N_w \rangle = \rho_0 V N_A / M_0$, where $\rho_0 = 1.0 \text{ g/cm}^3$ is the bulk water density, $M_0 = 18 \text{ g/mol}$ is the molar mass of water, and N_A is the Avogadro constant. Thus, we can write out a more general form of eq 4 as

$$Q = \frac{2D\rho_0 V N_A}{M_0 L^2} \quad (5)$$

However, for the present channel, because the predicted occupancy $\langle N_w \rangle = \rho_0 V N_A / M_0 = 125.3$ is clearly lower than the simulated result, the water flow given by eq 5 will be underestimated. Although $\langle N_w \rangle$ is not strictly proportional to V for small channels,¹⁸ it is likely that the linear relation between water occupancy and channel volume becomes more reliable for wider channels and thus eq 5 will yield a good estimate.

3.2. Charge Density and Patterns. Although eq 4 implicitly contains the channel dimension, clearly its pitfall is that it only considers the confinement effect of channel while neglecting the water-channel interactions. The water-channel interactions often play an important role in the transport

properties.^{6,35–37} Herein, when the channel becomes hydrophilic, i.e., it is charged, eq 4 fails and we should take into account the water-channel interactions. Figure 2 shows the

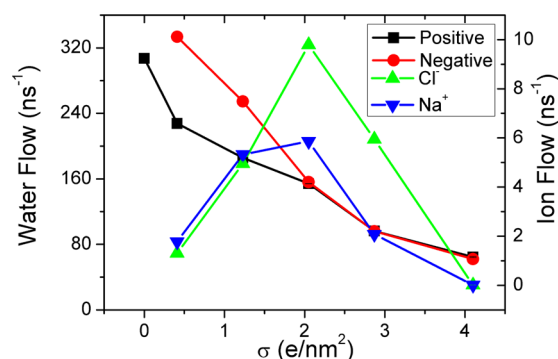


Figure 2. Water and ion flow as a function of the charge density for positively and negatively charged channels, respectively. Error bars are shown for two data points and are smaller than the symbols.

water flow as a function of charge density. The water flow decreases monotonously with the increase of charge density for both positively and negatively charged channels, indicating that the motion of water molecules inside charged channels is subjected to larger friction at a higher charge density. This result also supports that rapid conduction of water inside CNTs is codetermined by strong water–water and weak water–CNT interactions,⁸ which will be further discussed from the free energy profiles in the following. We also note that for the positive and negative channels, the water flow data nearly fall on top of each other at high charge densities $\sigma \geq 2.05$ e/nm², while they show large discrepancies for $\sigma < 2.05$ e/nm². This may be due to different hydrations of cations and anions,⁴¹ and/or different water-channel interactions. As Cl[−] has a greater hydration number than Na⁺, when it is adsorbed onto the interior surface of positive channel, the water flow can be affected more obviously. Also, as the oxygen atom is almost the center of mass of the water molecule and it has two times greater negative charge than the hydrogen atom, inside the positive channel, the electrostatic adsorption of oxygen-channel should hinder the water motion more distinctly. At high charge density, both counterions and water molecules have strong interactions with channels; these differences for positive and negative channels become trivial, resulting in a similar water flow.

We should also point out that the water flow behaviors are thoroughly different from a previous work that changes water-channel Lennard-Jones (LJ) potentials to vary the channel hydrophilicity.³⁵ Their results showed that for $\epsilon < 0.075$ kcal/mol, the water flow increase drastically with the increase of ϵ ; while for $\epsilon > 0.075$ kcal/mol, the flow achieves saturation and does not change appreciably with further increase of ϵ (up to 0.2 kcal/mol). Actually, when the interaction strength of the LJ potential is at a very small value, the water-channel interaction is almost purely repulsive, thus water molecules cannot enter the channel and the flow is close to zero. With the increase of the LJ interaction strength, water molecules prefer to enter the channel much more, leading to the increase of flow.

As we focus on the effect of charge density and patterns in the current study, our LJ potential is just fixed as the water–carbon parameters ($\epsilon = 0.1143$ kcal/mol) taken from the pioneering work of Hummer et al.⁶ which is widely used in

subsequent studies.^{8–10,21,24,25} Clearly, the water flow through the pristine CNT channel should be at the maximum plateau according to Melillo et al.³⁵ Since the electrostatic attraction is always several times larger than the LJ potential, the increase of channel charge will drastically increase the water-channel attraction, and thus increase the roughness of free energy profiles, leading to the decrease of water flow. It can be expected that for the channel without modified charge, if we further increase ϵ (>0.2 kcal/mol), the water flow should also decrease from the plateau. In another way, it is also believed that if we use $\epsilon < 0.075$ kcal/mol, a small amount of surface charges may facilitate entry of water, leading to the increase of water flow, and further increase of charge may also lead to the decrease of water flow. These opinions perhaps motivate future studies.

Briefly, we have discussed the water flow through charged channels. It still remains difficult to analytically include water-channel interactions in eq 4. From the decreasing water flow, the diffusion coefficient is expected to be decreased with the increase of charge density. Actually, in the following we will show that the water occupancy $\langle N_w \rangle$ is also dependent on the charge density. Thus, the water flow should be a complex nonlinear function of charge density, and future study is required to determine their relationships. As shown in Figure 2, we also presented the ion flow as a function of charge density. Remarkably, the ion flow has a maximum at the moderate charge density of $\sigma = 2.05$ e/nm² for both Cl[−] and Na⁺. This result should be due to the competition between ion number and ion-channel interaction. With the increase of σ , to neutralize the system, the counterion number is increased, and also the ion-channel attraction increases. At low charge density of $\sigma \leq 2.05$ e/nm², most of the ions inside the channel are mobile (discussed later); thus, the increasing ion number leads to the increase of ion flow. However, for $\sigma > 2.05$ e/nm², the ion-channel interaction becomes dominant, where ions should encounter large friction, since they are trapped in energy minima due to the spatial dependence on ion-channel interaction. Thus, the ion flow decreases with the further increase of σ . In particular, at $\sigma = 4.10$ e/nm², the ions are almost frozen on the channel surface, and we only observed three translocation events for both Cl[−] and Na⁺. At $\sigma = 2.05$ and 2.87 e/nm², the flow of Na⁺ is clearly smaller than Cl[−]; since Na⁺ has smaller LJ diameter and lower hydration number, it can be adsorbed onto the channel more easily.

In some experiments,^{29–33} different surface charge patterns can be achieved inside microfluidic channels. To further understand the effect of charge patterns on the water transport, for a given charge density of $\sigma = 2.05$ e/nm² we changed the percentage of charged atoms (PCA), and all the results are presented in our Supporting Information. As shown in Figure S2, the water and ion flows are clearly dependent on the PCA. As a whole, the water and ion flows decrease with the decrease of PCA. With the decrease of PCA, the charge amount of charged atoms increases; thus, the charged atoms have more attraction with water molecules and ions, leading to the decrease of their flows. However, there exists a sudden increase of water flow for the negative channel at small PCA, which should be related to the abrupt change of ions and will be discussed later. Compared to the water flow, the ion flow is more sensitive to the charge pattern, since the ion has net opposite charge, where the flow decreases several times with PCA. Especially at PCA = 0.05, the Na⁺ flow is completely zero. The asymmetric flow of Cl[−] and Na⁺ can be ascribed to their

different LJ diameter and hydration number. From these results we can conclude that, given for the same charge density, the charge patterns also have a nontrivial impact on the water and ion conduction.

In an effort to further elucidate the dynamics of water and ions inside charged channels, we show in Figure 3(a) their

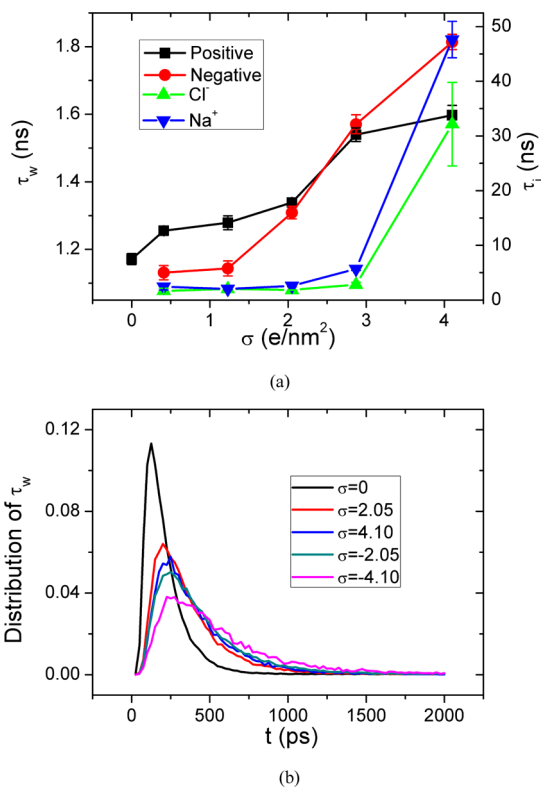


Figure 3. (a) Average translocation time of individual water molecules τ_w and ions τ_i , and (b) distributions of τ_w for different charge densities. Error bars in (a) are shown for two data points and are not shown in (b) for clarity.

translocation time as a function of charge density. τ_w for water increases nonlinearly with the increase of charge density, and this supports the decrease of water flow in Figure 2. At low σ , τ_w is relatively smaller for the negative channel, being in accordance with its larger flow value. However, at high σ , even the water flows are similar; τ_w becomes the larger one for the negative channel. Actually, at $\sigma = 4.1 \text{ e}/\text{nm}^2$, the water flows are $64.6 \pm 0.7 \text{ ns}^{-1}$ and $62.2 \pm 0.7 \text{ ns}^{-1}$ for the positive and negative channels, respectively. It is unclear whether such a minor flow difference is coupled to the τ_w difference, but we should point out that the distribution of τ_w is very wide, especially for high σ , just as seen in Figure 3(b), where the long tails after 2000 ps are not shown for clarity. As we have just discussed for the pristine CNT above, although the τ_w of most water molecules is only several hundreds of picoseconds, parts of them can be up to tens of nanoseconds. Remarkably, with the increase of σ , the distribution of τ_w becomes wider, implying that the number of water molecules that have large τ_w is increased. This is because, at high σ , the water molecules adsorbed onto the channel surface will encounter a large free energy barrier due to the channel charges and adsorbed ions, and have difficulty escaping from local minimas (discussed later). At $\sigma = 4.1 \text{ e}/\text{nm}^2$, τ_w has a wider distribution for the negative channel compared with the positive counterpart, which

may lead to its larger average value. The translocation time for ion τ_i is not very sensitive to σ at low σ , while it increases drastically at high σ . Actually, we only observed three translocation events for both Cl^- and Na^+ at $\sigma = 4.1 \text{ e}/\text{nm}^2$, where the ions are almost frozen on the channel surface. The translocation events of ions are not as sufficient as water; thus, the distribution of τ_i is not considered further. If we use $\langle N_w \rangle / \tau_w$ for the estimation of water flow through charged channels, we can get good agreement only at $\sigma = 2.87 \text{ e}/\text{nm}^2$ for the positive channel and $\sigma = 2.05 \text{ e}/\text{nm}^2$ for the negative channel, the largest discrepancy from simulated flow can be 0.5 times. As τ_w is sensitive to the small portion of water that has large translocation times, the estimation of $\langle N_w \rangle / \tau_w$ may not yield to reliable water flow.

We plotted PCA dependence of τ_w and τ_i , and the distribution of τ_w in Figure S3 of our Supporting Information. As a whole, the changes of τ_w and τ_i are in concert with the flow behaviors in Figure S2. As the value change of τ_w with PCA is not so large that the τ_w distribution is not very sensitive to PCA. Previous works showed the sensitivity of water occupancy with the change of water-channel LJ potentials,^{6,35} where large LJ interaction strength always leads to the increase of occupancy. However, surprisingly, the case becomes very different for the charged channels. As seen in Figure 4(a), for the negative

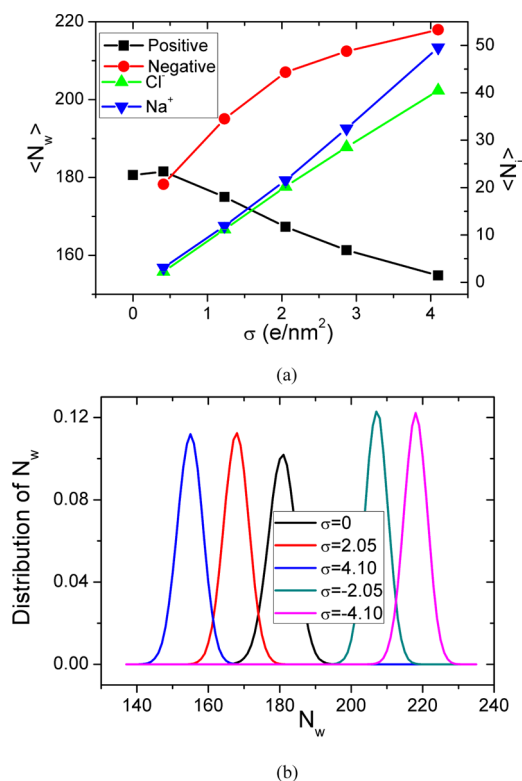


Figure 4. (a) Water and ion occupancy and (b) distributions of water occupancy for different charge densities. Error bars in (a) are smaller than the symbols, and are not shown in (b) for clarity.

channel, the increase of $\langle N_w \rangle$ with increasing charge density can be well understood in the context of the water-channel interaction, similar to the LJ potential case.^{6,35} Abnormally, for the positive channel $\langle N_w \rangle$ decreases with the increase of σ . This result should be caused by the squeeze of counterions. Actually, the average of $\langle N_w \rangle$ for positive and negative channels is very close to the value of pristine CNT. As also shown in

Figure 4(a), the ion occupancy increases linearly with σ . This can be well understood, since $\langle N_i \rangle$ should be proportional to the surface charge of the channel, i.e., $\langle N_i \rangle \sim \pi\sigma RL$, where R and L are the channel diameter and length, respectively. The values for Cl^- and Na^+ are similar at low σ , and split at high σ . Although with the increase of σ , the water-channel interaction increases, the increasing number of counterions will occupy more channel space. Meanwhile, water molecules can also be adsorbed by counterions. Thus, there should be a complex competition among the water–channel, water–ion, and ion–channel interactions, which codetermines the water occupancy. Clearly, according to previous work,⁴¹ Cl^- has larger LJ diameter than Na^+ ; thus, the excluded volume effect of Cl^- should be more obvious, which then leads to the decrease of $\langle N_w \rangle$ inside the positive channel. At high charge density of $\sigma = 4.1 \text{ e/nm}^2$, the occupancy of Na^+ is visibly larger than Cl^- . As Na^+ has smaller LJ diameter, under such a high charge density, the $\text{Na}^+ - \text{Na}^+$ repulsion can be overcome more easily by Na^+ –channel attraction than that of Cl^- , resulting in larger Na^+ occupancy.

To further understand the competition between ion size and charge, we inserted the size and mass of Cl^- as normal Na^+ for the positive channel, and vice versa for the negative channel. We conducted 25 ns MD runs with the last 20 ns for occupancy analysis. As the 20 ns MD trajectory contains 40000 independent samples when counting the occupancy, it should be enough to draw a qualitative comparison. As shown in Figure S4(a) of the Supporting Information, to our surprise, the water occupancy varies in the opposite direction for the small Cl^- and large Na^+ , compared to the normal Cl^- and Na^+ , respectively. While the values for the positive channel with normal Cl^- and negative channel with large Na^+ , and vice versa, are close to each other, respectively. Thus, the ion size plays a key role in determining the water occupancy, which should be more dominant than the charge. A similar phenomenon can also be seen at high σ for the ion occupancy, shown in Figure S4(b). At $\sigma = 4.1 \text{ e/nm}^2$, for normal ions, $\langle N_i \rangle$ of Na^+ is larger than Cl^- ; however, $\langle N_i \rangle$ of small Cl^- becomes the larger one, indicating the ion size is the dominant factor. Although these simulations with modified ion size do not correspond to real experiments, they are helpful to separate and identify the effects of charge vs excluded volume. It is believed that the ion size should also affect the transport dynamics of water, but to test this idea large amounts and long times of MD runs are required, which is beyond the scope of this paper.

We also presented the occupancy distribution of water for different σ in Figure 4(b). The peak location shifts to low and high values for the positive and negative channels, respectively, which is in accordance with Figure 4(a). Remarkably, the distribution is symmetric and Gaussian, which is first discussed by Hummer et al. forming the basis of many theories of the hydrophobic effect.⁴⁷ The peak value and width are not very sensitive to σ , and for $\sigma = 0, \pm 2.05, \pm 4.1 \text{ e/nm}^2$, the occupancy ranges are 160–198, 152–184, 137–170, 191–223, and 203–235, respectively. Recently, Patel et al. discussed the fluctuations of water near hydrophobic/hydrophilic surfaces and found long tails in the occupancy distribution,⁴⁸ which is different from the current results. In the Supporting Information, Figure S5(a) gives the PCA dependence of water and ion occupancy. It seems that the changes of $\langle N_w \rangle$ and $\langle N_i \rangle$ are coupled to each other. For the positive channel, with the decrease of PCA, $\langle N_w \rangle$ only slightly decreases, and inverse change can be seen for $\langle N_i \rangle$. However, there exists a sudden

decrease and increase for $\langle N_w \rangle$ and $\langle N_i \rangle$, respectively, for the negative channel at low PCA, which should be responsible for the similar sudden changes of flow and translocation time in Figure S2 and Figure S3(a), respectively. At low PCA, the charge amount of charged atoms becomes larger, as Na^+ has smaller LJ diameter and hydration number, the likelihood of its adsorption should be increased. This is supported by the zero flow at low PCA in Figure S2. The larger number of Na^+ may expel out more water molecules, resulting in the sudden decrease of $\langle N_w \rangle$. Meanwhile, greater electrical field from the channel can be screened by Na^+ , and water can flow more freely, explaining the sudden change in Figure S2 and Figure S3(a). The distributions in Figure S5(b) accompany the results of Figure S5(a).

The surface charges can affect the adsorption of counterions, and the thickness of EDL layers can also be changed. Thus, it will be interesting to see the distribution of ions inside the charged channels. Figure 5(a) shows the radial density profiles

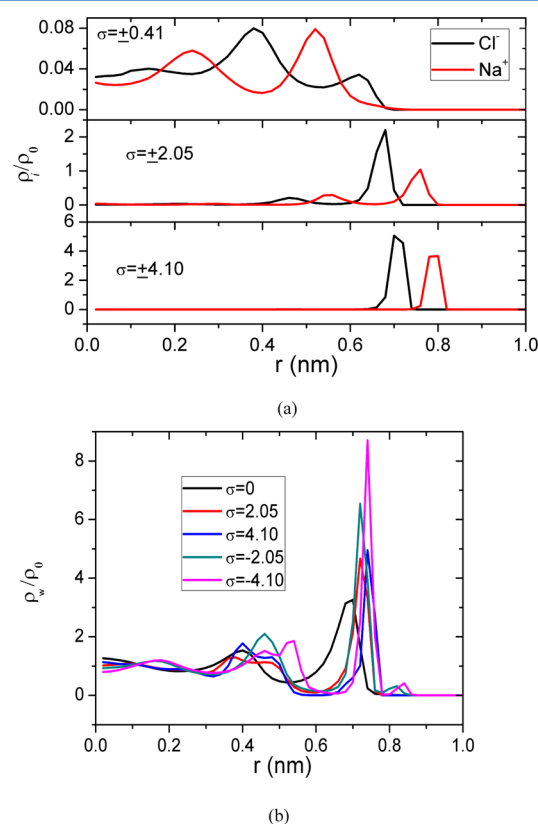


Figure 5. Radial density profiles of (a) ion and (b) water as a function of the radial distance from channel center. ρ_0 is the bulk water density and fixed as 1.0 g/cm^3 . Error bars are not shown for clarity.

for ions under different σ . There are two remarkable peaks for Cl^- and Na^+ at $\sigma = 0.41 \text{ e/nm}^2$, respectively, indicating ion layers. Actually, under such a low σ , the ions can be found anywhere inside the channel, since the density has a nonzero value anywhere, and the two peaks are relatively wide with low peak values. At $\sigma = 2.05 \text{ e/nm}^2$, the peaks clearly shift to the channel surface, and the main peak becomes sharp with high peak value, while a low peak is still visible. It should be noted that, for $r < 0.4 \text{ nm}$, the density is nonzero, and fluctuates between 0.01 and 0.03, with a small peak at $r = 0.22 \text{ nm}$ (peak value 0.029) and $r = 0.28 \text{ nm}$ (peak value 0.032) for Cl^- and Na^+ , respectively. At $\sigma = 4.1 \text{ e/nm}^2$, there is a single visible peak

and shifts to surface further with even higher peak value. However, the density of Cl^- is still nonzero for $r < 0.6$ nm, and fluctuates between 3×10^{-4} and 4×10^{-3} , with two peaks at $r = 0.22$ nm (peak value 0.001) and $r = 0.46$ nm (peak value 0.004); while the density of Na^+ is completely zero except for a very small peak (peak value 2×10^{-4}) between $r = 0.48$ – 0.6 nm.

If we connect the ion density distribution to the flow behavior in Figure 2, we can understand the dynamics of the ion more clearly. As the ion flow has a maximum at $\sigma = 2.05$ e/nm², and most ions are distributed on the first shell of channel surface, all the ions inside the channel should be mobile; otherwise, if the first shell ion is frozen, the small portion of ion left cannot generate such a large flow. Assuming all the ions inside the channel are mobile, we can further estimate the ion flow by $\langle N_i \rangle / \tau_i$, similar to the above water flow, but we should use the translocation time instead of diffusion time, since the ion moves near the charged surface, not in bulk water. At $\sigma = 2.05$ e/nm², for Cl^- , $\tau_i \sim 1.8$ ns and $\langle N_i \rangle \sim 20$, thus the ion flow is ~ 11 ns⁻¹, close to the simulated flow of ~ 10 ns⁻¹, suggesting that most ions inside the channel are mobile, which is further confirmed by observing the MD trajectory directly. For higher σ , the ions become closer to the channel surface and thus encounter larger friction, where the increase of τ_i exceeds that of $\langle N_i \rangle$, leading to the decrease of ion flow. At $\sigma = 4.1$ e/nm², the ions are almost frozen on the channel surface.

To further understand the water distributions, we show in Figure 5(b) the radial density profiles of water for different σ . The obvious peaks at $r = 0.4$ and 0.7 nm indicate water layers near the hydrophobic channel surface. Remarkably, with the increase of σ , the peaks shift to the channel surface due to the strong electrostatic attraction. Especially for the negative channel, the main peak near the surface becomes extremely high, where the peak value of $\sigma = -4.1$ e/nm² is almost twice larger than $\sigma = 4.1$ e/nm². This should be due to a different water arrangement near the positive and negative surface, similar to different hydration numbers of cations and anions.⁴¹ We also note that, for the same σ value, the location of the main peak is the same for the positive and negative channels, which is different from the ions. This is because Cl^- and Na^+ have different LJ diameters and hydration number. We further considered the effect of charge patterns on the density profiles, presented in Figure S6 of our Supporting Information. Clearly, the radial density of ion and water can be affected by the charge patterns, but is less remarkable than by the charge density.

To explore the physical reason responsible for the water flow behavior, we show in Figure 6 the free energy profiles as a function of the water position along the channel. We only consider the water at the first hydration shell of the channel surface, and according to Figure 5(b), the radial range can be chosen as $r = 0.6$ – 0.9 nm. From $\sigma = 0$ to $\sigma = \pm 2.05$ e/nm², the increase of roughness is not very remarkable. This is because the density fluctuation inside the current wide channel is not as large as the single-file waters inside narrow CNTs.³⁷ The strong confinement effect of narrow CNTs and the steric distribution of CNT atoms will lead to more obvious wave-like behaviors in the water axial density. With the further increase of σ , the roughness of the free energy curve increases remarkably. Especially for $\sigma = 4.1$ e/nm², there are large local energy barriers and minima, and water molecules have to constantly escape from one minimum to fall into another so as to move. Thus, the water will encounter higher effective friction, and the water flow can be decreased remarkably. In addition, the water-

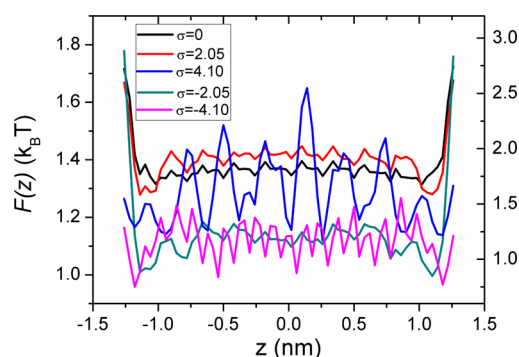


Figure 6. Free energy profiles $F(z) = -k_B T \ln[\rho(z)/\rho_0]$ for water at the first hydration shell of the channel interior surface (nm $0.6 < r < 0.9$ nm) as a function of the water position along the channel axis. Error bars are not shown for clarity. The data of $\sigma = 0, \pm 2.05$ e/nm² correspond to the left y-axis, and the data of $\sigma = \pm 4.10$ e/nm² correspond to the right y-axis.

channel (electrostatic and hydrophobic) interactions can also prevent water molecules from leaving, especially those having saturated hydrogen bonds inside the channel.

3.3. Channel Diameters. Up to now, we have discussed the effect of surface charge density and its pattern on the transport properties of water molecules through a relatively wide channel. For pristine CNT channels, the transport properties are often dependent on the channel size.^{17,18} Herein, we further investigated the channel size effect for a fixed charge density of $\sigma = 2.05$ e/nm², and we only considered uniformly charged channels due to the available computational resource. Figure 7 shows the flow, occupancy, and translocation times of water and ion as a function of the channel diameter, as well as the water structures inside pristine and charged channels with $R = 0.81$ nm. For $R = 0.81$ nm, the water flow is completely zero for the positive channel, while it is only 0.58 ± 0.15 ns⁻¹ for the negative channel; the ion flow is completely zero for both channels. These results can be connected to the specific water–ion structures inside the charged channels.

It is well-known that the water molecules inside the pristine CNT with $R = 0.81$ nm should exhibit single-file structure.^{6–10} However, inside the charged channel, the single-file structure is disrupted by the channel charge and counterions, demonstrated in Figure 7(d). The counterions insert between water molecules to form new hydrogen-bonded systems. Especially for the positive channel, the water–ion structure is unique, where one Cl^- inserts between two waters to form two H-bonds with the two nearby hydrogen atoms. This is because Cl^- has large LJ diameter, and it cannot occupy the same cross plane with a water molecule. Inside such a narrow channel Cl^- is surrounded by more channel atoms than the above wide one. Thus, it has a propensity to be trapped in local energy minima and is almost frozen, confirmed by observing the MD trajectory. As no water can slip with Cl^- , the water flow is completely zero. However, as seen in Figure 7(d), inside the negative channel, Na^+ can occupy the same cross plane with water due to its smaller LJ diameter. Thus, although it should be difficult, water still has some little chance to slip with Na^+ , leading to the small amount of water flow. Similarly, Na^+ is also very steady inside the channel.

As shown in Figure 7(a), excluding the first data point, with the increase of channel diameter, the water flow increases nonlinearly, following a power law scaling; while the ion flow increases almost linearly. The water flow overlaps for positive

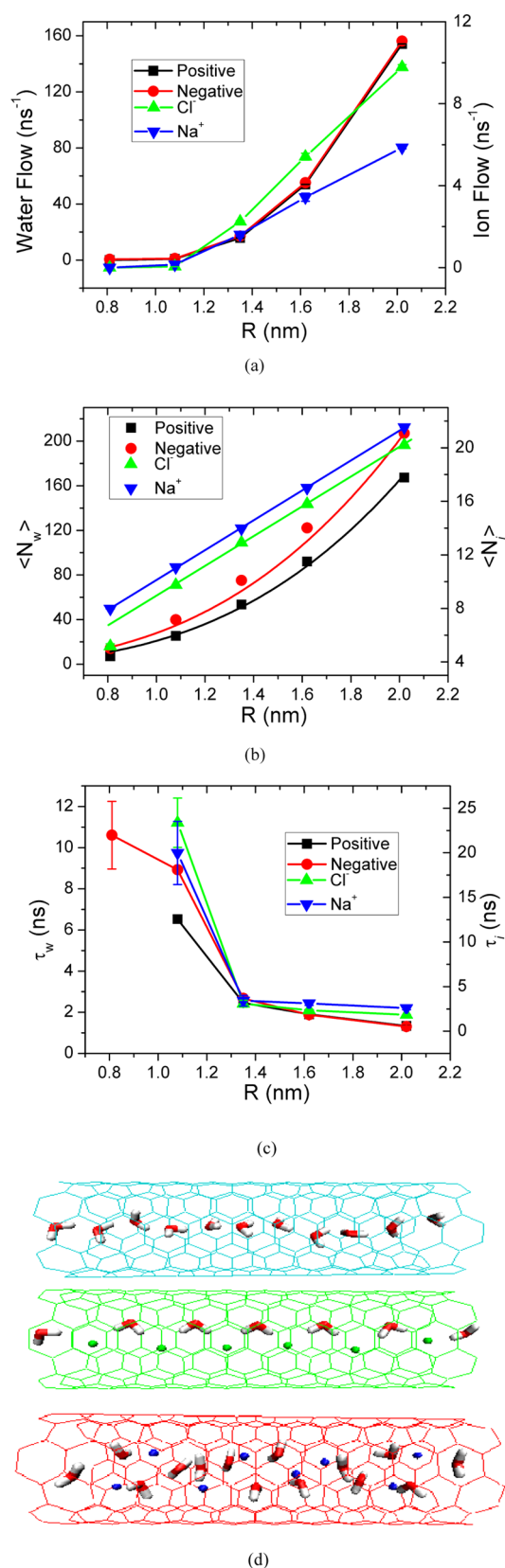


Figure 7. (a) Flow, (b) occupancy, and (c) translocation time of water and ions as a function of the channel diameter. (d) Water structure inside narrow ($R = 0.81$ nm) channels: from top to bottom are the pristine, positive, and negative channels, respectively. Error bars are shown for two data points. Lines in (b) are power law (for water) and linear (for ion) fittings for the same color data.

and negative channels, while the ion flow splits, which is similar to the above wide channel. The flow behaviors should be related to the similar occupancy behaviors, presented in Figure 7(b), where $\langle N_w \rangle$ and $\langle N_i \rangle$ exhibit power law and linear variations, respectively. For the positive and negative channels, the power law exponents are 2.90 ± 0.12 and 2.58 ± 0.10 , respectively, comparable with 2.73 for the pristine CNTs in a previous work.¹⁸ As has been discussed,¹⁸ if the water occupancy is proportional to the channel volume, the exponent should be 2. The larger exponents should be relevant to the finite-size effect of the channels. Both the $\langle N_w \rangle$ and $\langle N_i \rangle$ splits for positive and negative channels, due to the excluded volume effect of counterions, similar to the wide channel above. Also similar to the above wide channel, the average of $\langle N_w \rangle$ for positive and negative channels is very close to that of pristine CNTs with the same diameter. Clearly, the linear increase of ion occupancy is due to the linear increase of channel surface charge ($\pi\sigma RL$). The translocation time for both water and ion exhibits a sudden decrease with the increase of R for $R < 1.4$ nm, and decreases slightly with R further increases. This is because, inside small channels, ions could have strong ion-channel attraction, and thus they will be trapped in large local free energy minima, which also hinders the water conduction. In a word, the dynamics of water and counterions inside the charged channel is complex and should be coupled to each other.

4. CONCLUSION

In summary, we have investigated the permeation of water molecules through a charged channel by molecular dynamics simulations. For the pristine CNT channel without charges, we suggested an analytical expression, consisting of water diffusion coefficient, water occupancy and channel dimension, to predict the water flow. We discussed its rationality as well as pitfalls, and we may further explore it in the future works. We then concentrated on a relatively wide channel with various surface charge densities and patterns, and also discussed the results of channel size effect. For uniformly charged channels, with the increase of charge density σ , the water flow decreases monotonously, due to the increase of roughness in the free energy profile experienced by a water molecule along the channel. The ion flow has a clear maximum at an intermediate σ because of the competition between ion number and ion-channel attraction. We also analyzed the nonlinear translocation time and its distributions. The water occupancy for the negative channel increases with σ , while surprisingly, it varies in the opposite direction for the positive channel. This result should mainly stem from the excluded volume effect of ions, as evidenced by the results of artificially changing the size of cation and anion to be same. The symmetric and Gaussian distributions of water occupancy are similar to the case of pristine CNT. The radial density profiles of ion and water are split according to σ . Along with these results, the charge pattern effect is considered, wherein similar dynamic and thermal dynamic properties are presented. We finally investigated the channel size effect, where we found some interesting water dynamics and structures in a narrow channel. In a word, the transport properties of water through charged channels become much more complex than hydrophobic channels, which should be coupled to the counterions. Through this work, our understanding of the transport properties of hydrophilic channels can be improved significantly, which is particularly helpful for the design of nanofluidic devices.

■ ASSOCIATED CONTENT

■ Supporting Information

The charge patterns and results of pattern effect. This material is available free of charge via the Internet at <http://pubs.acs.org>.

■ AUTHOR INFORMATION

Corresponding Author

*E-mail: jysu@iccas.ac.cn; hxguo@iccas.ac.cn. Phone: 86-10-82618124.

Notes

The authors declare no competing financial interest.

■ ACKNOWLEDGMENTS

This work is financially supported by the National Science Foundation of China (21204093, 21174154, 20874110) and Chinese Academy of Sciences (KJCX2-YW-H19). The allocated computer time at the Supercomputer Center of Chinese Academy of Sciences is gratefully acknowledged.

■ REFERENCES

- (1) De Groot, B. L.; Grubmüller, H. Water Permeation across Biological Membranes: Mechanism and Dynamics of Aquaporin-1 and GlpF. *Science* **2001**, *294*, 2353–2357.
- (2) Agre, P. Aquaporin Water Channels (Nobel Lecture). *Angew. Chem. Int. Edn.* **2004**, *43*, 4278–4290.
- (3) García-Fandiño, R.; Sansom, M. S. P. Designing Biomimetic Pores Based on Carbon Nanotubes. *Proc. Natl. Acad. Sci. U.S.A.* **2012**, *109*, 6939–6944.
- (4) Majumder, M.; Chopra, N.; Andrews, R.; Hinds, B. Nanoscale Hydrodynamics: Enhanced Flow in Carbon Nanotubes. *Nature* **2005**, *438*, 44–44.
- (5) Holt, J.; Park, H.; Wang, Y.; Stadermann, M.; Artyukhin, A.; Grigoropoulos, C.; Noy, A.; Bakajin, O. Fast Mass Transport Through Sub-2-Nanometer Carbon Nanotubes. *Science* **2006**, *312*, 1034–1037.
- (6) Hummer, G.; Rasaiah, J.; Noworyta, J. Water Conduction Through the Hydrophobic Channel of a Carbon Nanotube. *Nature* **2001**, *414*, 188–190.
- (7) Joseph, S.; Aluru, N. R. Why are Carbon Nanotubes Fast Transporters of Water? *Nano Lett.* **2008**, *8*, 452–458.
- (8) Rasaiah, J. C.; Garde, S.; Hummer, G. Water in Nonpolar Confinement: From Nanotubes to Proteins and Beyond. *Annu. Rev. Phys. Chem.* **2008**, *59*, 713–740.
- (9) Fang, H. P.; Wan, R. Z.; Gong, X. J.; Lu, H. J.; Li, S. Y. Dynamics of Single-File Water Chains inside Nanoscale Channels: Physics, Biological Significance and Applications. *J. Phys. D: Appl. Phys.* **2008**, *41*, 103002.
- (10) Kofinger, J.; Hummer, G.; Dellago, C. Single-file Water in Nanopores. *Phys. Chem. Chem. Phys.* **2011**, *13*, 15403–15417.
- (11) Kofinger, J.; Hummer, G.; Dellago, C. Macroscopically Ordered Water in Nanopores. *Proc. Natl. Acad. Sci. U.S.A.* **2008**, *105*, 13218–13222.
- (12) Koga, K.; Gao, G. T.; Tanaka, H.; Zeng, X. C. Formation of Ordered Ice Nanotubes inside Carbon Nanotubes. *Nature* **2001**, *412*, 802–805.
- (13) Bai, J. E.; Wang, J.; Zeng, X. C. Multiwalled Ice Helices and Ice Nanotubes. *Proc. Natl. Acad. Sci. U.S.A.* **2006**, *103*, 19664–19667.
- (14) Cambré, S.; Schoeters, B.; Luyckx, S.; Goovaerts, E.; Wenseleers, W. Experimental Observation of Single-File Water Filling of Thin Single-Wall Carbon Nanotubes down to Chiral Index (5,3). *Phys. Rev. Lett.* **2010**, *104*, 207401.
- (15) Wang, H. J.; Xi, X. K.; Kleinhammes, A.; Wu, Y. Temperature-Induced Hydrophobic–Hydrophilic Transition Observed by Water Adsorption. *Science* **2008**, *322*, 80–83.
- (16) Cambré, S.; Wenseleers, W. Separation and Diameter-Sorting of Empty (End-Capped) and Water-Filled (Open) Carbon Nanotubes by Density Gradient Ultracentrifugation. *Angew. Chem., Int. Ed.* **2011**, *50*, 2764–2768.
- (17) Thomas, J. A.; McGaughey, A. J. H. Reassessing Fast Water Transport Through Carbon Nanotubes. *Nano Lett.* **2008**, *8*, 2788–2793.
- (18) Su, J. Y.; Guo, H. X. Effect of Nanochannel Dimension on the Transport of Water Molecules. *J. Phys. Chem. B* **2012**, *116*, 5925–5932.
- (19) Corry, B. Water and Ion Transport Through Functionalised Carbon Nanotubes: Implications for Desalination Technology. *Energy Environ. Sci.* **2011**, *4*, 751–759.
- (20) Kalra, A.; Garde, S.; Hummer, G. Osmotic Water Transport Through Carbon Nanotube Membranes. *Proc. Natl. Acad. Sci. U.S.A.* **2003**, *100*, 10175–10180.
- (21) Gong, X. J.; Li, J. C.; Xu, K.; Wang, J. F.; Yang, H. A Controllable Molecular Sieve for Na⁺ and K⁺ Ions. *J. Am. Chem. Soc.* **2010**, *132*, 1873–1877.
- (22) Yeh, I. C.; Hummer, G. Nucleic Acid Transport Through Carbon Nanotube Membranes. *Proc. Natl. Acad. Sci. U.S.A.* **2004**, *101*, 12171–12182.
- (23) Bhirde, A. A.; Patel, V.; Gavard, J.; Zhang, G. F.; Sousa, A. A.; Masedunskas, A.; Leapman, R. D.; Weigert, R.; Gutkind, J. S.; Rusling, J. F. Targeted Killing of Cancer Cells in Vivo and in Vitro with EGF-Directed Carbon Nanotube-Based Drug Delivery. *ACS Nano* **2009**, *3*, 307–316.
- (24) Tu, Y. S.; Xiu, P.; Wan, R. Z.; Hu, J.; Zhou, R. H.; Fang, H. P. Water-Mediated Signal Multiplication with Y-Shaped Carbon Nanotubes. *Proc. Natl. Acad. Sci. U.S.A.* **2009**, *106*, 18120–18124.
- (25) Li, J. Y.; Gong, X. J.; Lu, H. J.; Li, D.; Fang, H. P.; Zhou, R. H. Electrostatic Gating of a Nanometer Water Channel. *Proc. Natl. Acad. Sci. U.S.A.* **2007**, *104*, 3687–3692.
- (26) Vaitheeswaran, S.; Rasaiah, J. C.; Hummer, G. Electric Field and Temperature Effects on Water in the Narrow Nonpolar Pores of Carbon Nanotubes. *J. Chem. Phys.* **2004**, *121*, 7955–7964.
- (27) Su, J. Y.; Guo, H. X. Control of Unidirectional Transport of Single-File Water Molecules Through Carbon Nanotubes in an Electric Field. *ACS Nano* **2011**, *5*, 351–359.
- (28) Liu, B.; Li, X. Y.; Li, B. L.; Xu, B. Q.; Zhao, Y. L. Carbon Nanotube Based Artificial Water Channel Protein: Membrane Perturbation and Water Transportation. *Nano Lett.* **2009**, *9*, 1386–1394.
- (29) Schoch, R. B.; Han, J.; Renaud, P. Transport Phenomena in Nanofluidics. *Rev. Mod. Phys.* **2008**, *80*, 839–883.
- (30) Duan, C.; Majumdar, A. Anomalous Ion Transport in 2-nm Hydrophilic Nanochannels. *Nat. Nanotechnol.* **2010**, *5*, 848–852.
- (31) Vlassioulis, I.; Kozel, T. R.; Siwy, Z. S. Biosensing with Nanofluidic Diodes. *J. Am. Chem. Soc.* **2009**, *131*, 8211–8220.
- (32) He, Y.; Gillespie, D.; Boda, D.; Vlassioulis, I.; Eisenberg, R. S.; Siwy, Z. S. Tuning Transport Properties of Nanofluidic Devices with Local Charge Inversion. *J. Am. Chem. Soc.* **2009**, *131*, 5194–5202.
- (33) Siwy, Z. S.; Howorka, S. Engineered Voltage-Responsive Nanopores. *Chem. Soc. Rev.* **2010**, *39*, 1115–1132.
- (34) Goldsmith, J.; Martens, C. C. Molecular Dynamics Simulation of Salt Rejection in Model Surface-Modified Nanopores. *J. Phys. Chem. Lett.* **2010**, *1*, 528–535.
- (35) Melillo, M.; Zhu, F. Q.; Snyder, M. A.; Mittal, J. Water Transport Through Nanotubes with Varying Interaction Strength between Tube Wall and Water. *J. Phys. Chem. Lett.* **2011**, *2*, 2978–2983.
- (36) Yang, Y. L.; Li, X. Y.; Jiang, J. L.; Du, H. L.; Zhao, L. N.; Zhao, Y. L. Control Performance and Biomembrane Disturbance of Carbon Nanotube Artificial Water Channels by Nitrogen-Doping. *ACS Nano* **2010**, *4*, 5755–5762.
- (37) Li, X. Y.; Shi, Y. C.; Yang, Y. L.; Du, H. L.; Zhou, R. H.; Zhao, Y. L. How Does Water-Nanotube Interaction Influence Water Flow Through the Nanochannel? *J. Chem. Phys.* **2012**, *136*, 175101.
- (38) Su, J. Y.; de la Cruz, M. O.; Guo, H. X. Solubility and Transport of Cationic and Anionic Patterned Nanoparticles. *Phys. Rev. E* **2012**, *85*, 011504.

- (39) Lindahl, E.; Hess, B.; van der Spoel, D. GROMACS 3.0: A Package for Molecular Simulation and Trajectory Analysis. *J. Mol. Model.* **2001**, *7*, 306–317.
- (40) Jorgensen, W. L.; Chandrasekhar, J.; Madura, J. D.; Impey, R. W.; Klein, M. L. Comparison of Simple Potential Functions for Simulating Liquid Water. *J. Chem. Phys.* **1983**, *79*, 926–935.
- (41) Chowdhuri, S.; Chandra, A. Hydration Structure and Diffusion of Ions in Supercooled Water: Ion Size Effects. *J. Chem. Phys.* **2003**, *118*, 9719–9725.
- (42) Essmann, U.; Perera, L.; Berkowitz, M. L.; Darden, T.; Lee, H.; Pedersen, L. G. A Smooth Particle Mesh Ewald Method. *J. Chem. Phys.* **1995**, *103*, 8577–8593.
- (43) Bussi, G.; Parrinello, M. Stochastic Thermostats: Comparison of Local and Global Schemes. *Comput. Phys. Commun.* **2008**, *179*, 26–29.
- (44) Yeh, I. C.; Hummer, G. System-Size Dependence of Diffusion Coefficients and Viscosities from Molecular Dynamics Simulations with Periodic Boundary Conditions. *J. Phys. Chem. B* **2004**, *108*, 15873–15879.
- (45) Milischuk, A. A.; Branka, M.; Ladanyi, B. M. Structure and dynamics of water confined in silica nanopores. *J. Chem. Phys.* **2011**, *135*, 174709.
- (46) Cheng, L.; Morrone, J. A.; Berne, B. J. Structure and Dynamics of Acetonitrile Confined in a Silica Nanopore. *J. Phys. Chem. C* **2012**, *116*, 9582–9593.
- (47) Hummer, G.; Garde, S.; Garcia, A. E.; Pohorille, A.; Part, L. R. An Information Theory Model of Hydrophobic Interactions. *Proc. Natl. Acad. Sci. U.S.A.* **1996**, *93*, 8951–8955.
- (48) Patel, A. J.; Varilly, P. V.; Chandler, D. C. Fluctuations of Water near Extended Hydrophobic and Hydrophilic Surfaces. *J. Phys. Chem. B* **2010**, *114*, 1632–1637.